

Modeling Sea Ice Thickness using Machine Learning and Remote Sensing Modalities

John Baker

Ira A. Fulton Schools of Engineering

School of Computing and Augmented Intelligence

APPROVED:

Dr. Douglas Cochran _____, Director

Dr. Hua Wei _____, Second Reader

ACCEPTED:

Dean, Barrett, the Honors College

ARIZONA STATE UNIVERSITY

Modeling Sea Ice Thickness using
Machine Learning and Remote
Sensing Modalities

HONORS THESIS
BARRETT, THE HONORS COLLEGE

Author:
John Baker

Committee:
Dr. Douglas Cochran
Dr. Hua Wei

April 2024

Acknowledgement

I hereby declare that I can carry out the present work independently without outside help. and used only the sources and aids indicated. I assure Furthermore, that I have not yet submitted this thesis to any other examination board.

Abstract

Little is known about the state of Arctic sea ice at any given instance in time. The harshness of the Arctic naturally limits the amount of in-situ data that can be collected, resulting in gathered data being limited in both location and time. Remote sensing modalities such as Synthetic Aperture Radar (SAR) imaging and laser altimetry help compensate for the lack of data, but suffer from uncertainty because of its inherent indirectness. Furthermore, precise remote sensing modalities tend to be severely limited in spatial and temporal availability, while broad methods are more accessible at the expense of precision. This thesis focuses on the intersection of these two problems and explores the possibility of corroborating remote sensing methods to create a precise, accessible source of data that can be used to examine sea ice at a local scale.

Contents

1	Introduction	4
2	Data Collection	9
2.1	SAR Imaging	9
2.2	Laser Altimetry (IceSat-2)	11
3	Experimentation	14
3.1	Setup	14
3.2	Model Results	16
4	Discussion	18
4.1	Limitations	18
4.2	Practical Implications	19
4.3	Future Work	19
5	Conclusion	20
5.1	Research Questions	20
List of Figures		21
A	Appendix A: ATL10 Product	i

Introduction

In recent decades, understanding the state of sea ice has grown increasingly important. Sea ice analysis at large scales can provide valuable insight into the trajectory of climate change and at local scale has implications in fields like arctic navigation. Understanding sea-ice thickness in particular, is important for both of these applications. For example, the thickness of the ice can be analyzed over time to track ice mass in relation to global warning or interpreted locally to predict shipping speed through ice-covered water [1].

Due to the harsh nature of the arctic, in-situ studies of arctic ice are infrequent both in time and space. Thus, most analyses depend heavily on remote sensing methods. These methods cumulatively provide magnitudes more data than in-situ measurements can achieve, but differ in modality, methodology and resolution. Synthetic Aperture Radar (SAR) and light detection and ranging (LiDAR) are some such modalities that survey the arctic region.

Organizations like the National Aeronautics and Space Administration (NASA) and European Space Agency (ESA) freely provide this information through their constellation of satellites.

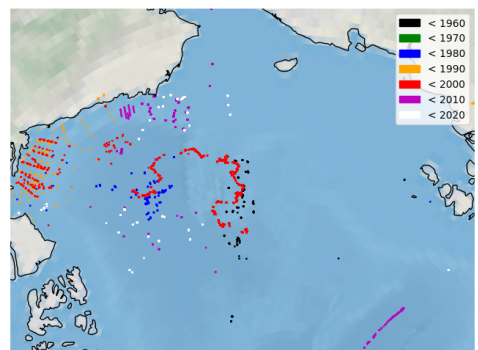


Figure 1.1: Historic In-Situ Data Availability in the Beaufort Sea Region

Each of these remote sensing methods have their individual strengths and limitations. ICESat-2 (IS-2), a NASA LiDAR satellite, features 6 separate lasers and works by emitting individual photons and timing their respective returns. Praised for its precision, its readings are statistically corrected to adjust for ambient light, cloud occlusion (atmospheric scattering), snow and ice scattering, and the physical problem of first-photon bias [2]. Its lasers have a ground-surface footprint of 17 meters, demonstrating how local its sampling is. IS-2's statistical robustness offers valuable local observation with less than 5 meters of total geolocation error (mean $+1\sigma$) [3].

In contrast to IS-2's highly accurate and local measurements, SAR imaging offers significantly more expansive data with a loss in local precision. SAR images Earth's surface by emitting radio waves and then reconstructing the surface composition based upon the return signal. The physical difference between photons and radio waves means that LiDAR's limitations with occlusion are actually imperceptible to SAR satellites. Radio waves permeate clouds and snow, and the reconstructed image is independent of light [4]. These weather independent properties make SAR an excellent modality to monitor sea ice especially during winter seasons, with satellites like Sentinel-2 (SN-2) from the ESA offering 290 kilometer swaths of imaging, at resolutions ranging between 10 and 60 meters [5]. It's important to note that despite its extensiveness, SAR is more sensitive to physical factors like surface roughness, slant, and type, and also suffers from speckle noise [4].

Given the availability of remote sensed data and their different observed properties, there is much to be learned about the state of the sea ice by corroborating these data sources with each other. Uniquely, the corroboration of a SAR image with precise LiDAR measurements suggests the possibility of developing a convolutional neural network (CNN) to accurately predict

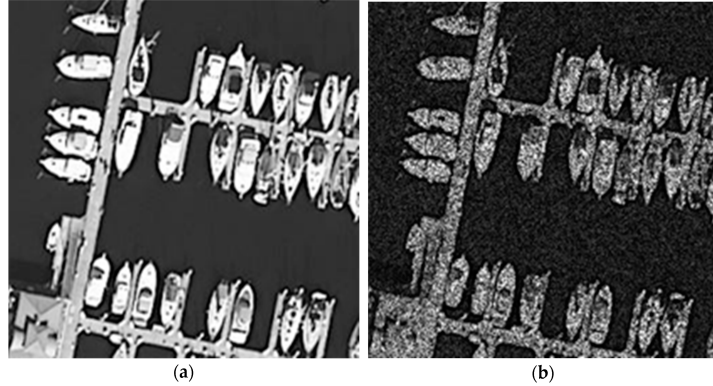


Figure 1.2: a. Optical Image; b. SAR Image with speckle noise

sea ice thickness using expansive SAR imaging. Doing so successfully would effectively map IS-2’s precision onto the weather agnostic, extensive imaging gathered by SAR satellites, thus allowing for local scale analysis of sea ice across large regions.

Given that ice thickness is not a property directly measured by LiDAR nor captured in SAR imagery, sets of assumptions need to be made to deduce the property through related measurements. A leading paradigm in modeling ice thickness is through the assumption of hydrostatic equilibrium [6]–[8], in which the properties of the ice sheet are deduced based upon the fact that the ice is buoyant in sea water (Figure 1.3). In this assumption, LiDAR measurements retrieve the elevations of the snow covered ice-surface in relation to the sea surface, and statistically infer the sea ice surface height. It’s possible to relate the ice’s total thickness to these elevation measurements by combining these relative heights with their associated substance densities (Equation 1.1). NASA’s IS-2 L4 Along-Track Sea Ice Thickness product is a closely related example of this topic, and produced arctic ice thickness results between October 2018 and May 2022 [6].

Major critiques of the hydrostatic model stem from its assumption of

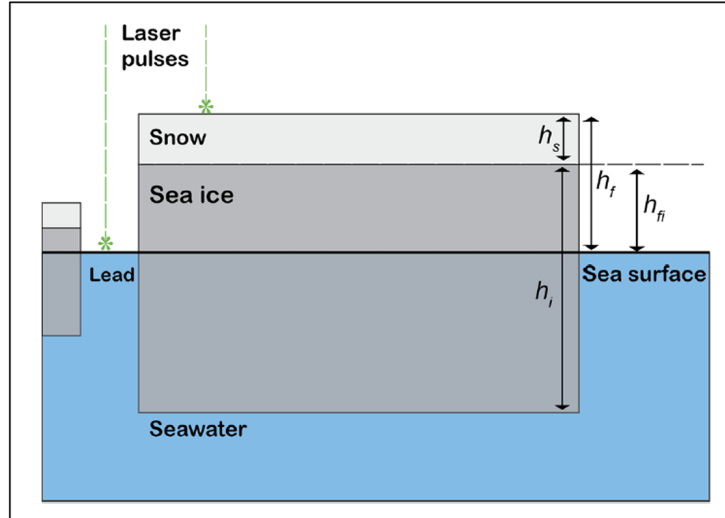


Figure 1.3: Ice Thickness Isostatic Assumption
[6]

the innately variable densities of snow and ice. Ice density is dependent on factors like salinity, temperature, air volume and exposure [1] which all vary across local scales. The differences in ice quality are significant enough that SAR imaging is already capable of segmenting images into their first and multi-year components [9]. Some studies delineate ice density by whether it's above or below the waterline, but find that air-rich above water ice only contributes to 10% of the total density of the ice sheet. Given the variability, the exact local density of sea ice in the remote arctic is ephemeral, but generally agreed upon to be between $900\text{-}940 \frac{kg}{m^3}$, with some studies proposing a slightly wider range of 892-945 [1]. As concrete examples for density though, IS-2's L4 product settled to use a value of $916 \frac{kg}{m^3}$ for ice above and below the waterline and $1024 \frac{kg}{m^3}$ for sea water. Arctic snow density differs from ice density as it is more uniform across the arctic, but varies seasonally across the winter and summer months [10]. Reasonable values range between $210 \frac{kg}{m^3}$ in August, to $310 \frac{kg}{m^3}$ in June [10].

$$h_i = \frac{h_f \rho_w}{(\rho_w - \rho_i)} + \frac{h_s (\rho_s - \rho_w)}{(\rho_w - \rho_i)} \quad (1.1)$$

where:

$$\begin{aligned} h_i &= \text{Sea ice thickness (m)} & \rho_i &= \text{Density of sea ice } (900 - 940 \frac{\text{kg}}{\text{m}^3}) \\ h_s &= \text{Snow depth (m)} & \rho_s &= \text{Density of snow } (210 - 310 \frac{\text{kg}}{\text{m}^3}) \\ h_f &= \text{Freeboard height (m)} & \rho_w &= \text{Density of water } (1024 \frac{\text{kg}}{\text{m}^3}) \end{aligned}$$

Even with the established hydrostatic model in place to infer sea ice thickness from remote sensing methods, there is an innate problem with the corroboration of SAR and LiDAR. IS-2 has an orbit cycle of 91 days, meaning each location is surveyed only once nearly every 3 months [2], while SN-2 orbits nearly once every 5 days [11]. It may appear that there should be plenty of data available given the semi-frequent opportunity for coincidence, but given SN-2's best resolution of 10m, any correlation with IS-2's 17m footprint leads to single pixels of information.

The remainder of the thesis will be split between discussing the data collection and machine learning model experimentation. The data collection section will discuss the procedure for obtaining datasets of interest, as well as some intermediate efforts done to promote accuracy. The experimentation will use the collected data to develop a convolutional neural network to explore the feasibility of using such a source of data for deep learning models.

Data Collection

The data collection portion of this project is immediately tasked with the following set of problems: spatial coincidence, temporal coincidence, and resolution. Given the asynchronous orbits of each satellite and the incompatible resolutions of ESA's SN-2 and NASA's IS-2, other avenues were explored to obtain precise SAR imaging. Of note were NASA's "ICESAT-2" mobile application and ICEYE's[©] SAR imaging offered through the ESA. The ICESAT-2 mobile application tracks IS-2's footprint location and lists the dates and times of the next times the satellite will fly over a position. ICEYE is a third party satellite provider through the ESA that offers "SPOT" and "SLEA" SAR imaging products, featuring 1m resolution and extent ranging from 1km^2 to 15km^2 [12]. The appeal of ICEYE's 1m resolution products is that a nominal acquisition of its SPOT data product would coincide with ≈ 350 unique IS-2 footprints while the SLEA product would coincide with ≈ 5300 .

2.1 SAR Imaging

ICEYE's superior resolution is significantly more compatible with IS-2's small footprint, but is not made freely available as it's a private company. However, they are a participant in the ESA's Third Party Missions Program, meaning the ESA can sponsor the data delivery through their Earth

Observation User Services Portal.

To achieve ESA sponsorship of this data, a proposal was submitted including the objective of the project, researchers involved in the task, which satellite and product was being requested, and a general plan outlining the use of the sponsored data. Given the latency of proposal approval, and the seasonal characteristics of arctic sea ice, interim efforts were made to coincide freely available SN-2 10m resolution data with IS-2's altimetry.

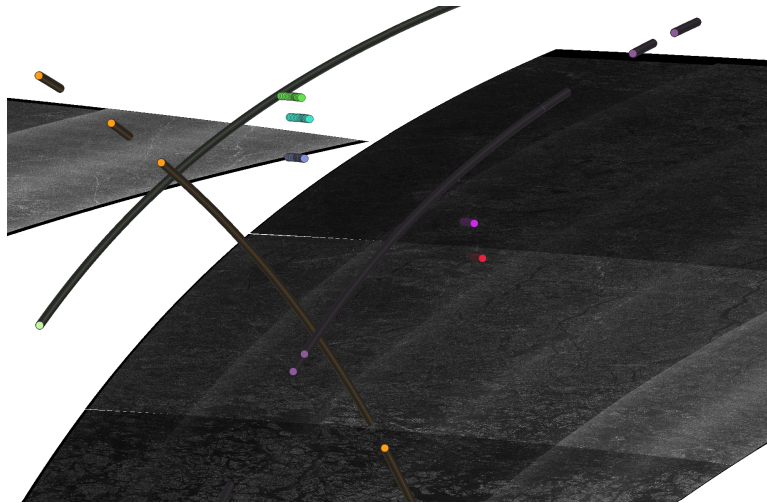


Figure 2.1: Near-Coincidence of SN-2 and IS-2, February 20-21 2023

Referring to ESA's Copernicus Open Access Hub and NASA's Earthdata Search tool, a near coincident set of SN-2 and IS-2 data was obtained for February 20-21 of 2023 (Figure 2.1). The SAR imaging clearly captured regions of arctic ice, and did so on February 20th at 4:50pm UTC. The predominantly spatially coincident IS-2 measurements, being the long purple and orange tracks in the figure, crossed the region at 10am and 10pm UTC on February 21. This data while immensely geographically coincident, was dubious because of its 17 and 29 hour respective temporal delay. Utility scripts were devised to track buoy movement in the area across the time period, and the nearest buoy (purple) to any of the tracks was 30 kilometers

away and had traveled another 8 km during the data's time difference. The corroboration of buoy movement in the area invalidates the possibility of the data being correlated, as it's unreasonable to account for the drift of the ice over the given time and space scale. While unsuccessful, this instance demonstrates the unavailability of naturally coincident data and the inefficiencies in obtaining it.

Later, the ESA approved the project proposal and agreed to sponsor 2 SPOT and 2 SLEA images. With this sponsorship, specific SAR imagery was then ordered that coincided with IS-2's flight path. In preparation for the data order, locations were selected in the ICESAT-2 mobile application and validated to have sea ice by viewing recent SN-2 data via Copernicus Open Access Hub. Then, an order form was submitted to ICEYE detailing the acquisition information to which they'd respond regarding its feasibility. This ordering and validation was repeated until all 4 sponsored images were fulfilled (Figure 2.2).

2.2 Laser Altimetry (IceSat-2)

The ICESAT-2 mobile application and ICEYE's flexibility handled the issues of spatial and temporal coincidence. IS-2 data was simply collected from the National Snow and Ice Data Center (NSIDC) repository after its own acquisition of the selected area. Each IS-2 acquisition offers multiple data products, but for the study of sea ice the ATL10 product is most relevant. The ATL10 data product contains inferences about sea-ice freeboard using data propagated from their ATL07 sea ice height product. Thus, a single ATL10 delivery contains the interpreted sea surface height, ice surface height, and the total freeboard [2] needed to infer sea ice thickness (Equation 1.1).

The recorded data is captured and delivered in a ".h5" file requiring

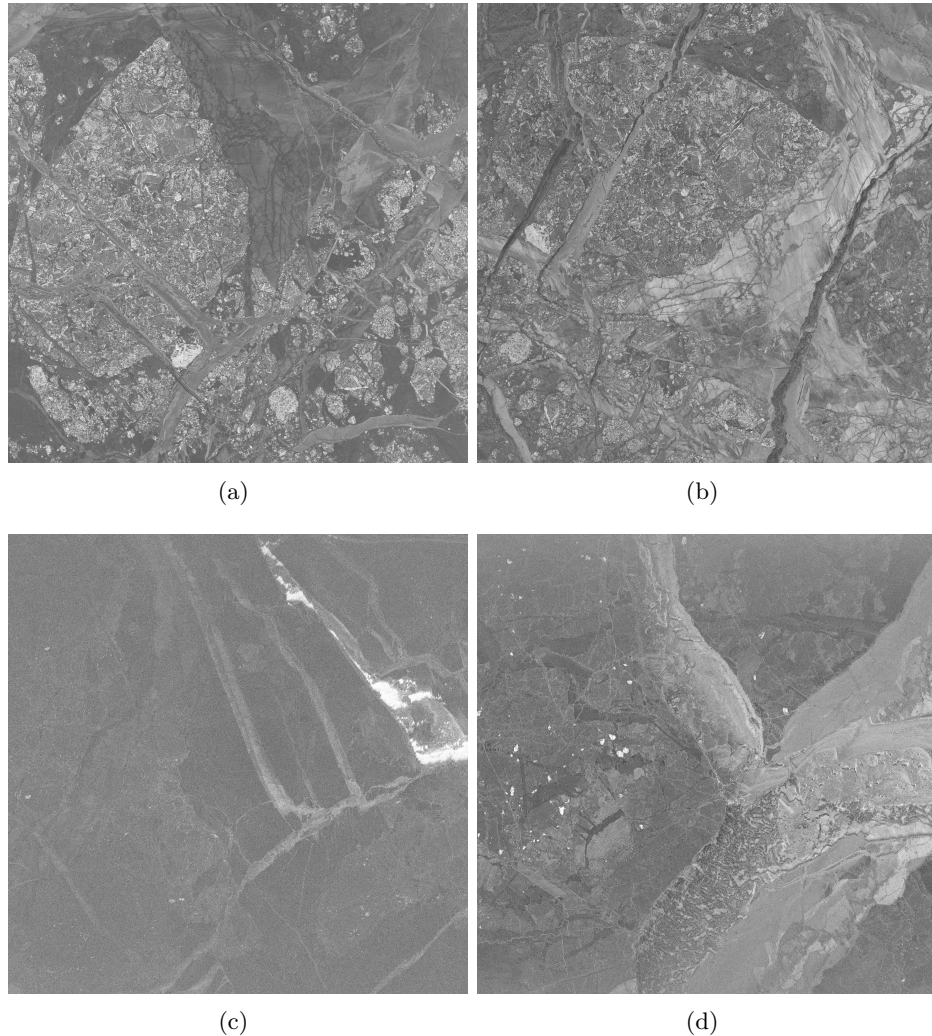


Figure 2.2:

- (a) SLEA 1/19 02:35:35 UTC (73.396, -141.668)
- (b) SLEA 1/19 04:40:35 UTC (73.395, -141.664),
- (c) SPOT 1/20 13:29:02 UTC (72.816, -133.975),
- (d) SPOT 1/20 20:25:52 UTC (72.816, -133.976)

parsing to extract relevant information. Appendix A contains a list of the fields that were extracted, and a brief description of each based upon the ATL10 data product specification [2].

After receiving the SAR imaging from ICEYE and the IS-2 data from the NSIDC, the best delivery was Figure 2.2b. Figure 2.2b was 6 minutes

coincident with the IS-2 track, thus offering the greatest source of ground truth. A severe limitation of the extracted data though, is that IS-2 omits data when it detects ice concentration $<50\%$. For this reason, the ATL10.h5 product for this acquisition only contained data from its GT2R and GT3R beams, effectively yielding 33% of the information initially expected. Figure 2.3 shows the intersecting IS-2 tracks, and figure 2.4 demonstrates the surface profile of the captured data, which will be used to interpolate ice thickness in future sections.

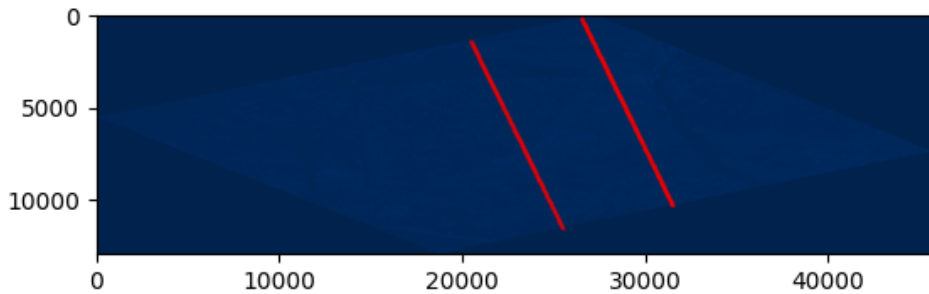


Figure 2.3: IS-2 Tracks across ICEYE Image

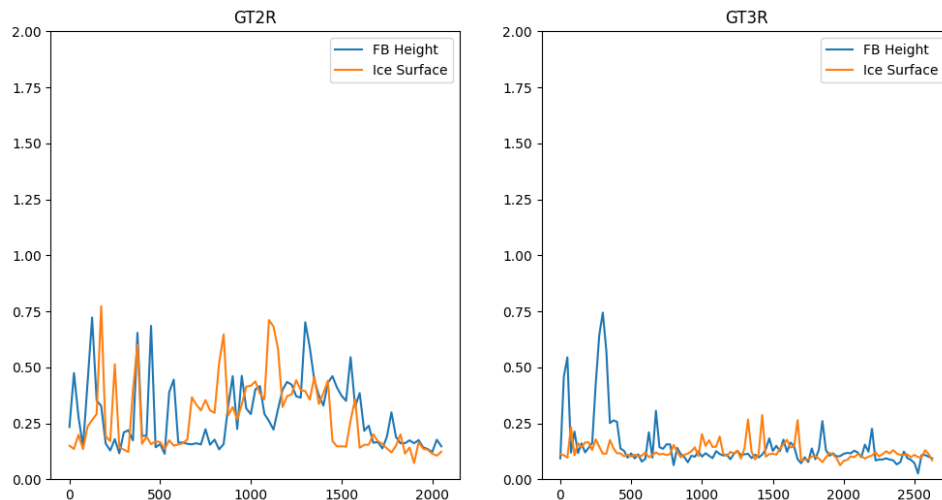


Figure 2.4: Ice Surface Profiles

Experimentation

The intuition behind developing a CNN on this dataset is novel. Many related works demonstrate the feasibility of using CNN models to classify or segment SAR imaging [9], but tend not to explore regression tasks. This could be the result of the unavailability of a public dataset like the one derived for this study. Furthermore, attempting to relate IS-2 footprints to high resolution SAR imaging involves deriving information from single-channel imagery of low pixel dimension. Compounded with the 33% yield of anticipated data from the ICEYE image, the limited data problem is exacerbated.

3.1 Setup

The coincident data is first extracted from the ICEYE imagery, yielding 4,683 17x17 tiles with associated LiDAR measurements. The selected densities used for interpolation are as follows, where the snow density is drawn from historical measurements during the month of January [10].

$$\begin{aligned}\rho_i &= \text{Density of sea ice } (916 \frac{kg}{m^3}) \\ \rho_s &= \text{Density of snow } (300 \frac{kg}{m^3}) \\ \rho_w &= \text{Density of water } (1024 \frac{kg}{m^3})\end{aligned}$$

Using Equation 1.1, each tile’s elevation readings are converted to their associated thickness. Some values of freeboard are negative, so they are interpreted to represent the absence of snow and an overestimate of sea ice surface elevation. The negative freeboard values are then added to the sea ice surface elevation to compensate. Each tile’s interpolated ice thickness can be visualized in Figure 3.1.

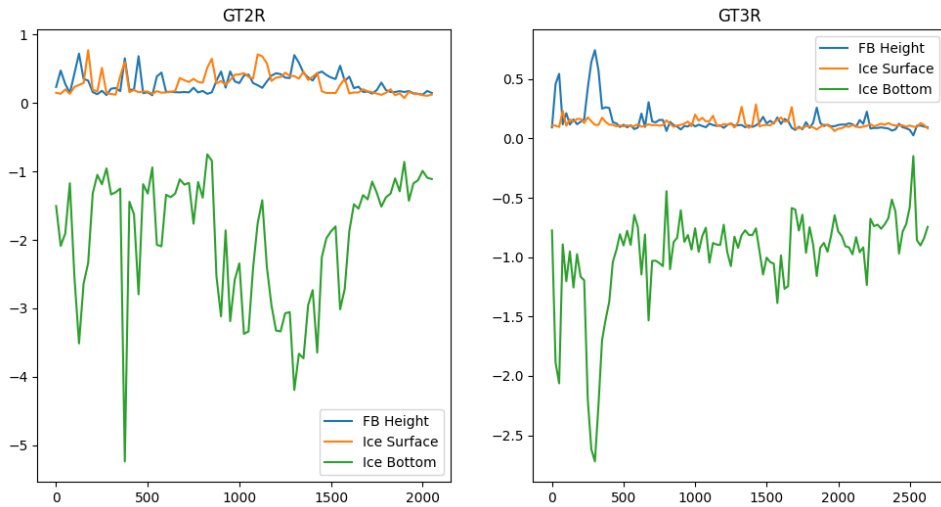


Figure 3.1: Interpolated Ice Thickness

The experimental model for the data is a feed forward neural network, consisting of 3 convolutional layers and 3 fully connected layers. Each convolutional layer is followed by the ReLU activation function, and the model uses the ADAM optimizer at a 10^{-5} learning rate based upon the L1 loss function. Given the already minimal pixel-space dimension, pooling and filter dilation are avoided to better preserve information across layers of the network.

The intuition behind experimenting with a simple model is rooted largely from the sparseness of existing studies attempting regression on low-resolution single channel images. Studies on classification, however, find that

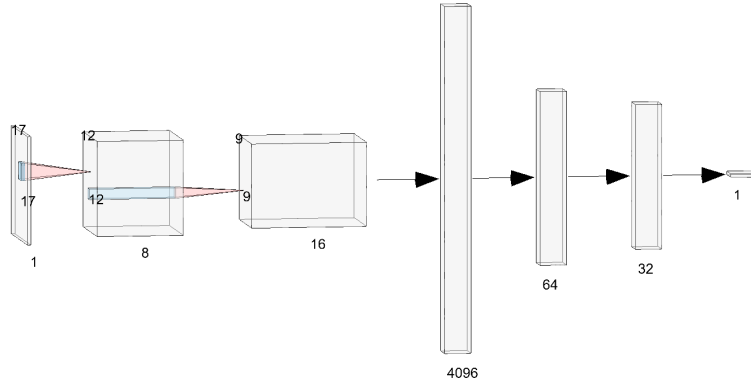


Figure 3.2: CNN Architecture

wider datasets (data that spans more classes) benefit from a larger amount of neurons in fully connected layers [13]. Regression tasks for continuous numbers can be thought of as infinite classification, thus supporting the decision to implement multiple fully connected layers of large dimension. Some classification studies find value in decreasing filter sizes with model depth [14], but for this model, kernel size is decreased from 5 to 3 only between the first and second convolution layer.

The training process for the model uses 80% of the data to train and 20% to test, a batch size of 32 to promote faster convergence, random flipping and rotation to prevent over-fitting, and scaling of each pixel to the [0,255] color range. The model is trained over 100 epochs.

3.2 Model Results

After 100 epochs, the model fails to converge (Figure 3.3). The L1 Loss function plateaus at ≈ 0.66 , and the model predicts a concentrated set of values slightly lower than the test set's mean. This value can be explained by the L1 Loss function's insensitivity towards outliers, as the mean (vertical bar) would be shifted right because of the skew in the input distribution.

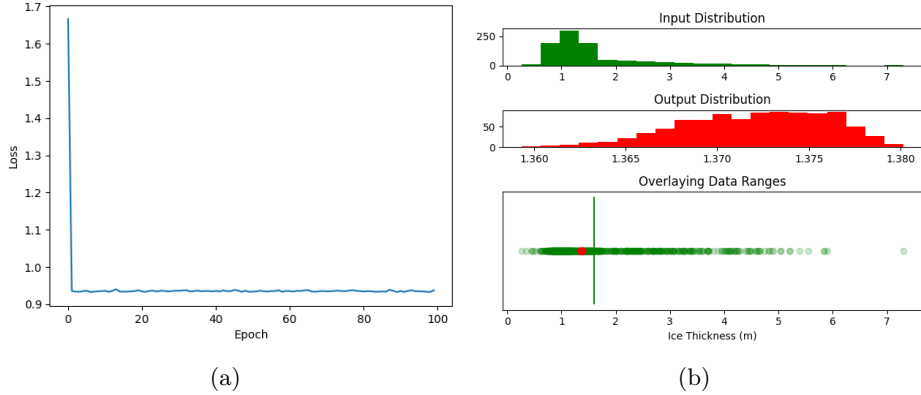


Figure 3.3: (a) Model Convergence (b) Model Predictions

The model reports an R2 value of -.056 and an RMSE of 0.9996, both of which suggest the model does not fit the data at all. The normalized RMSE is 0.14, which seemingly better, is only the result of the relatively narrow range of ice thicknesses being predicted in the testing set. Minor changes to the activation function and hyper-parameters yielded no significant difference to the model's evaluation metrics, nor did they assist in loss convergence. The inadequacies demonstrated by these tests suggest a more sophisticated architecture would be needed to better associate these low-resolution 1 channel images with their interpolated thickness measurements.

Discussion

In the Discussion section you should elaborate on the following points:

4.1 Limitations

While intuitive, the fundamental approach to this problem lies on a set of assumptions that may not always be true. At the root of the deduction of sea-ice thickness using IceSat-2 freeboard measurement is the assumption of hydro-static equilibrium at the measured footprint. The equation relies on the densities of snow, ice, and sea water, which are constants that may vary seasonally and geographically. Additionally, each footprint in this equation is assuming the absence of any other forces acting on the body. This thesis neither considered nor explored the dynamics of sea-ice floes, meaning that the calculated thickness at any given location may differ not only from error, but from a faulty equation derived from an incomplete physical understanding of the observed body.

- Luck of acquiring coincident data, even with project sponsorship - Even the 6 minutes coincident. No buoys are close enough to validate, but it only takes 3 meters per minute of movement to remove the coincidence from ICESAT-2's track. No way to know for this case. E.G. that's an assumption we made for the experimentation - Band specific SAR imaging (X-Band from ICEYE is different from SN-2) - Variable ranges of ice density - not entirely

sure what the right values are at any given moment in time - Hydrostatic assumption ignores other forces on the body from adjacent ice

4.2 Practical Implications

- Demo, does not need to be coded

4.3 Future Work

In the future, this topic can be further explored by examining different machine learning models and architectures that may be better suited on 2-channel, low-resolution imaging. To aid this, more data should be collected from both IceSat-2 and ICEYE.

Conclusion

The result of this thesis is a rough pipeline that links elusive data to a intuitive method of better modeling sea ice. IceSat-2's semi-frequent orbit provides data that can, with planning, be corroborated with other data sources to bridge the gap between different remote sensing methods. The results of the experimentation do not suggest the model is capable of deducing sea-ice thickness from mere SAR imaging.

5.1 Research Questions

Here you will answer your research questions, as they appear in the introduction. Answer each question in a different section. Relate your answer to your results. Discuss if your findings support and align with related work or not. Explain why do you think this happens, especially if your findings contradict existing work. Discuss alternative interpretations of your findings.

List of Figures

1.1	Historic In-Situ Data Availability in the Beaufort Sea Region	4
1.2	SAR Speckle Noise	6
1.3	Ice Thickness Isostatic Assumption	7
2.1	Existing Coincident Data Unavailability	10
2.2	ICEYE Captured SAR Imagery	12
2.3	Overlaid LiDAR and SAR Readings	13
2.4	Ice Surface Profile of Acquired Data	13
3.1	Interpolated Ice Thickness	15
3.2	CNN Architecture	16
3.3	Model Performance	17

Bibliography

- [1] G. Timco and W. Weeks, “A review of the engineering properties of sea ice”, *Cold Regions Science and Technology*, vol. 60, no. 2, pp. 107–129, 2010, ISSN: 0165-232X. DOI: <https://doi.org/10.1016/j.coldregions.2009.10.003>. [Online]. Available: <https://www.sciencedirect.com/science/article/pii/S0165232X09001797>.
- [2] K. R., A. A. Petty, G. Cunningham, *et al.*, *Atlas/icesat-2 l3a sea ice freeboard, version 6*, 2023. DOI: 10.5067/ATLAS/ATL10.006. [Online]. Available: <https://nsidc.org/data/ATL10/versions/6>.
- [3] T. Schenk, B. Csatho, and T. Neumann, “Assessment of icesat-2’s horizontal accuracy using precisely surveyed terrains in mcmurdo dry valleys, antarctica”, *IEEE Transactions on Geoscience and Remote Sensing*, vol. 60, pp. 1–11, 2022. DOI: 10.1109/TGRS.2022.3147722.
- [4] P. Singh, M. Diwakar, A. Shankar, R. Shree, and M. Kumar, “A review on sar image and its despeckling”, *Archives of Computational Methods in Engineering*, vol. 28, no. 7, pp. 4633–4653, 2021, ISSN: 1886-1784. DOI: 10.1007/s11831-021-09548-z. [Online]. Available: <https://doi.org/10.1007/s11831-021-09548-z>.
- [5] C. D. S. Ecosystem, *Sentinel-2 — dataspace.copernicus.eu*, <https://dataspace.copernicus.eu/explore-data/data-collections/sentinel-data/sentinel-2>, [Accessed 09-04-2024].

- [6] Petty, A. A., N. Kurtz, R. Kwok, T. Markus, and T. A. Neumann., *Icesat-2 l4 along-track sea ice thickness, version 1*, 2022. DOI: 10 . 5067/JTI5YG3S6VAJ. [Online]. Available: <https://nsidc.org/data/IS2SITDAT4/versions/1>.
- [7] J. K. Hutchings, P. Heil, O. Lecomte, R. Stevens, A. Steer, and J. L. Lieser, “Comparing methods of measuring sea-ice density in the east antarctic”, *Annals of Glaciology*, vol. 56, no. 69, 77–82, 2015. DOI: 10.3189/2015AoG69A814.
- [8] S. Forsström, S. Gerland, and C. A. Pedersen, “Thickness and density of snow-covered sea ice and hydrostatic equilibrium assumption from in situ measurements in fram strait, the barents sea and the svalbard coast”, *Annals of Glaciology*, vol. 52, no. 57, 261–270, 2011. DOI: 10.3189/172756411795931598.
- [9] Y. Huang, Y. Ren, and X. Li, “Classifying sea ice types from sar images using a u-net-based deep learning model”, in *2021 IEEE International Geoscience and Remote Sensing Symposium IGARSS*, 2021, pp. 3502–3505. DOI: 10.1109/IGARSS47720.2021.9554511.
- [10] S. G. Warren, I. G. Rigor, N. Untersteiner, *et al.*, “Snow depth on arctic sea ice”, *Journal of Climate*, vol. 12, no. 6, pp. 1814–1829, 1999.
- [11] *Sentinel-2 - Missions - Sentinel Online - Sentinel Online — sentinel.copernicus.eu*, <https://sentinels.copernicus.eu/web/sentinel/missions/sentinel-2>, [Accessed 11-04-2024].
- [12] *Types of SAR Data Products - ICEYE Product Documentation — sar.iceye.com*, <https://sar.iceye.com/5.2.5/productguide/sardataproducts/>, [Accessed 12-04-2024].

- [13] S. S. Basha, S. R. Dubey, V. Pulabaigari, and S. Mukherjee, “Impact of fully connected layers on performance of convolutional neural networks for image classification”, *Neurocomputing*, vol. 378, pp. 112–119, 2020, ISSN: 0925-2312. DOI: <https://doi.org/10.1016/j.neucom.2019.10.008>. [Online]. Available: <https://www.sciencedirect.com/science/article/pii/S0925231219313803>.
- [14] A. Ganj, M. Ebadpour, M. Darvish, and H. Bahador, *Lr-net: A block-based convolutional neural network for low-resolution image classification*, 2023. arXiv: 2207.09531 [cs.CV].

Appendix A: ATL10 Product

Field Name	Description
/freeboard_segment/latitude	ATL10 Data Product Columns
/freeboard_segment/longitude	ATL10 Data Product Columns
/freeboard_segment/beam_fb_height	ATL10 Data Product Columns
/freeboard_segment/beam_fb_confidence	ATL10 Data Product Columns
/freeboard_segment/beam_fb_quality	ATL10 Data Product Columns
/freeboard_segment/beam_fb_unc	ATL10 Data Product Columns
/freeboard_segment/beam_refsurf_ndx	ATL10 Data Product Columns
/freeboard_segment/height_segment_id	ATL10 Data Product Columns
freeboard_segment/seg_dist_x	ATL10 Data Product Columns
/freeboard_segment/heights/layer_flag	ATL10 Data Product Columns
/freeboard_segment/heights/ice_conc	ATL10 Data Product Columns
/freeboard_segment/heights/height_segment_1	ATL10 Data Product Columns
/freeboard_segment/heights/height_segment_2	ATL10 Data Product Columns
/freeboard_segment/heights/height_segment_3	ATL10 Data Product Columns
/freeboard_segment/heights/height_segment_4	ATL10 Data Product Columns
/freeboard_segment/heights/height_segment_5	ATL10 Data Product Columns
/reference_surface_section/beam_refsur	ATL10 Data Product Columns
/reference_surface_section/beam_refsur	ATL10 Data Product Columns
/reference_surface_section/beam_fb_unc	ATL10 Data Product Columns
/reference_surface_section/beam_refsur	ATL10 Data Product Columns
/reference_surface_section/beam_refsur	ATL10 Data Product Columns
/reference_surface_section/beam_refsur	ATL10 Data Product Columns